Fabrication and performance of TiN/TiAlN nanometer modulated coatings

Chang-Lin Liang [a,b], Guo-An Cheng [a,*], Rui-Ting Zheng [a], Hua-Ping Liu [a]

[a] Key Laboratory of Beam Technology and Material Modification of Ministry of Education, College of Nuclear Science and Technology, Beijing Normal University, Beijing 100875, China
[b] Department of Physics, Tsinghua University, Beijing 100084, China

ARTICLE INFO

ABSTRACT

TiN/TiAlN multilayered coatings with bilayer periods (λ_{BD}) ranging from 6 to 30 nm were prepared on TC4 alloy and Si (100) wafer substrates by magnetic filtered pulsed vacuum cathodic arc plasma technique. The analyses with scanning electron microscope (SEM), X-ray diffraction (XRD), X-ray energy dispersive spectroscope (EDS) and X-ray photoelectron spectroscope (XPS) with Ar + sputtering indicated that the as-deposited coatings had nanometer modulated structure, TiN and TiAlN with (111) preferred orientation were the main compounds and the average atoms ratio of N:(Ti + Al) was about 1.24–1.29. Scratch test showed that the coatings were fairly adherent to TC4 substrates, and the maximal critical load was about 57 N. The highest nano-hardness and modulus about 28 GPa and 283 GPa, respectively, were obtained for the multilayer with $\lambda_{BD} = 12$ nm, examined with nano-indentation method. The electrochemical corrosion test showed that the coatings improved the TC4 alloy's property of anti-corrosion effectively, especially with $\lambda_{BD} = 20$ nm.

© 2011 Elsevier B.V. All rights reserved.

1. Introduction

Transition metal nitrides were investigated widely due to their excellent intrinsic properties such as good conductivity, high hardness and wear resistance, being applied as diffusion barriers, hard or wear resistant coatings and anti-corrosion coatings [1–11]. Among these films, TiN, TiAlN and TiN or TiAlN based compounds are the most important materials for the well-comprehensive properties. However, TiN coating is readily oxidized and loses its valuable properties if the working temperature exceeds 500 °C. Though Al doping in TiN can improve the properties of corrosion and oxidation resistance at a high temperature, the disadvantages of TiAlN coating, such as the brittleness, weak adhesion and higher friction coefficient, restricted its extensive applications [3,6,7]. Fortunately, in recent years multi-layer or nanometer modulated coatings received great interest for very high hardness and toughness, a low level of residual stress, an inhibition for crack propagation and a high adhesion strength, pro-viding a promising approach to optimize enhance the performances of these coatings [4,8,9,12–26].

In this work, in order to study the techniques of synthesizing the properties of TiN and TiAlN, and moreover improving the perfor-mances of the coatings with nanometer period structures, we fabricated TiN/TiAlN multilayer coatings with different bilayer periods on Si (100) wafer and titanium alloy (TC4) substrates using magnetic filtered pulsed vacuum cathodic arc plasma technique, and charac-terized the coatings with scanning electron microscope (SEM), X-ray diffraction (XRD), X-ray energy dispersive spectroscope (EDS) and X-ray photoelectron spectroscope (XPS). The performances were also examined by nano-indentation, scratch test and electrochemical corrosion test.

2. Experiment

2.1. Coatings deposition

The deposition system is schematically shown in Fig. 1(a). It has a pair of cathodes, one is made of pure Ti (99.9%) and the other is made of TiAl alloy (Ti-47.5Al-2.5V-1Cr). They could work alternately. The DC voltage is applied between the cathode and the anode. When the chamber is evacuated, under the high voltage pulse triggering, the cathode arc occurred and create vast plasmas including electrons, ions, atoms and macro liquid drops of the cathode materials which diffuse to anode and enter into the bend transferring pipe. During transferring, the ions are restricted by the axial magnetic field created by the electric coil surrounding the pipe and move forward along the pipe, finally arrive at the specimen holder to deposit a film. But the neutral atoms or macro particles are not restricted by the field and directly go to the bend pipe inner wall, so they are filtered effectively. The film thickness is estimated with charge integration method which has been calibrated. The ultimate vacuum of the system is about 3.5×10^{-4} Pa.

TC4 alloy (Ti-6Al-4V) substrates had been ground and mirror-polished. Before being arranged on the sample holder, both Si (100) wafer and the TC4 substrates were ultrasonically cleaned in the analytically pure acetone and ethanol in turn, and then were air-dried. In the vacuum chamber, the substrate surfaces were further cleaned

* Corresponding author.
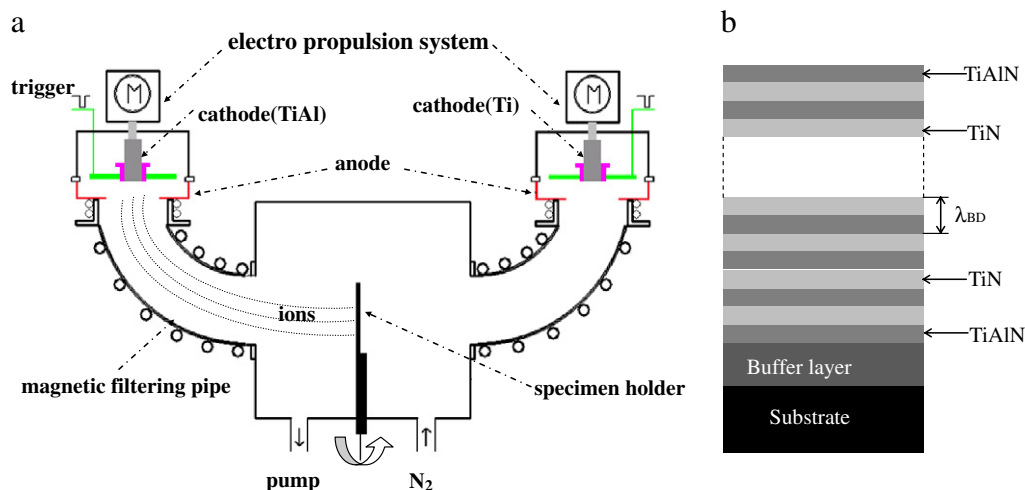E-mail address: gacheng@bnu.edu.cn (G.-A. Cheng).

Fig. 1. (a) The schematic diagram of the deposition system, (b) The schematic diagram of the coating structure.

by the energetic ions bombardment for 2 min due to the applied high bias voltage (DC −3 kV). While preparing the films the holder was biased with DC −100 V. The coating structure is schematically shown in Fig. 1(b). Firstly, a buffer layer of TiAl alloy with the thickness of about 100 nm was pre-deposited. Subsequently, nitrogen was injected into the chamber and reacted with the metal ions. By rotating the holder, TiN or TiAlN layers were prepared alternately at the ambient temperature. During nitrides deposition the chamber held the pressure of about $(4.0–4.4) \times 10^{-2}$ Pa with nitrogen gas flow of 12 sccm. The bilayer periods (λ_{BD}) were designed as to be 6, 12, 20 and 30 nm, corresponding to the bilayer numbers were 135, 65, 40 and 27, respectively. For each bilayer, the thickness of the sub-layer of TiN or TiAlN kept equally. In all cases, the first and the last layers were both TiAlN.

2.2. Coatings characterization

The cross-sectional morphologies of the as-deposited coatings were observed with SEM (Hitachi, S-4800), and at the same time the overall thicknesses of the coatings were estimated from these images indirectly. So, the bilayer period was estimated through the bilayer number dividing the thickness. Wide-angle XRD patterns of the coatings in Bragg-Brentano θ–2θ geometry were recorded in a diffractmeter (Rigaku, D/max-2400) with CuKα radiation ($\lambda = 0.15406$ nm). The elemental composition of the coating was examined with EDS (Hitachi S-4800). XPS (VG ESCALAB-5) equipped Ar^+ (2 keV) gun with the etching speed of about 1 nm/min was also used to investigate the chemical state and composition. The binding energy of the element was

obtained by a peak-fitting procedure using a Shirley background and mixed Gaussian–Lorentzian peak shape.

2.3. Performances examination

The nano-hardness and the elastic modulus measurements were performed in a nanoindenter (MTS, II) with the maximal load of 19 mN. Scratch test with the highest load of 100 N was used to detect the adhesion strength of the coatings to TC4 substrates, which was characterized by the critical load when the original damage occurred, which was indicated by acoustic signal emission. Potentiodynamic sweeping method with the Tafel technique was conducted to investigate the properties of electro-chemical corrosion for the coatings on TC4 substrates at room temperature in 3.5% aqueous NaCl solution. A saturated calomel electrode (SCE) was used to measure the potential across the electrochemical interface. The auxiliary electrode was platinum. The eroded area of the sample was limited to be about 28.27 mm^2.

3. Results and discussion

3.1. Microstructure and composition of the coatings

Fig. 2 exhibits the cross-sectional morphologies of the coatings with different bilayer periods on Si wafers by SEM. It can be seen that the coatings with lower λ_{BD} grew continuously. The growth manner was changed with λ_{BD} increasing. For the coatings with $\lambda_{BD} = 6$ and 12 nm, the texture is near equi-axed crystal grain and for the coating
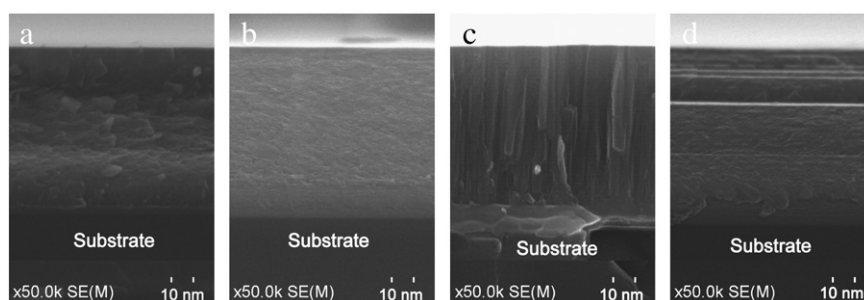

Fig. 2. Cross-sectional SEM images of the coatings on Si (100) wafers: (a) λBD = 6 nm, (b) λBD = 12 nm, (c) λBD = 20 nm, (d) λBD = 30 nm.
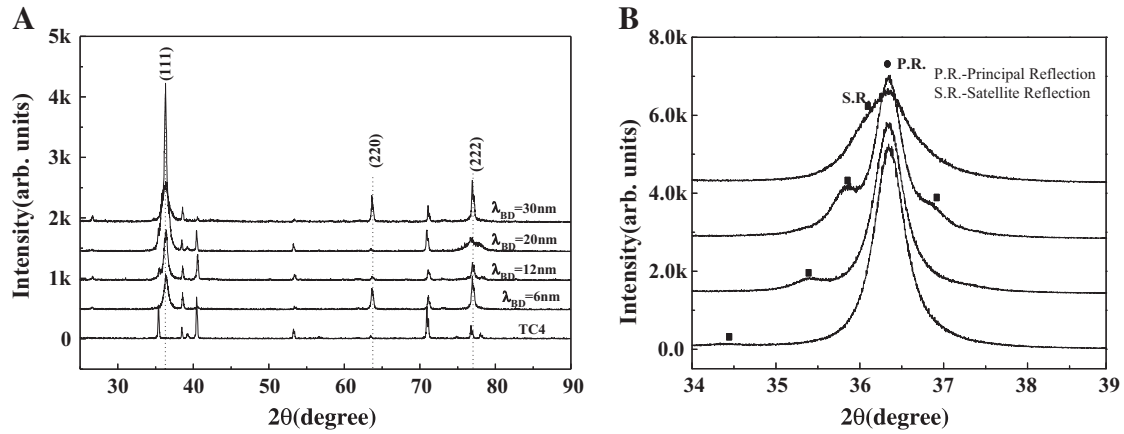
Fig. 3. XRD patterns from the coatings (a) on TC4 substrates (the peaks that are not indexed correspond to TC4 substrate), (b) on Si wafers.

with $\lambda_{BD} = 20$ nm it is columnar crystal. But for the coating with $\lambda_{BD} = 30$ nm at initial stage it grew in near equi-axed grain manner and then changed into columnar crystal manner, and moreover, delaminated. This might be caused by the inner strain increasing with the film growth. The coatings with near equi-axed grain morphology are very dense and might be beneficial to oxidation resistance by reducing the oxygen diffusion tunnels. Blurry fringes were found in the coating with $\lambda_{BD} = 20$ and in the top segment of the coating with
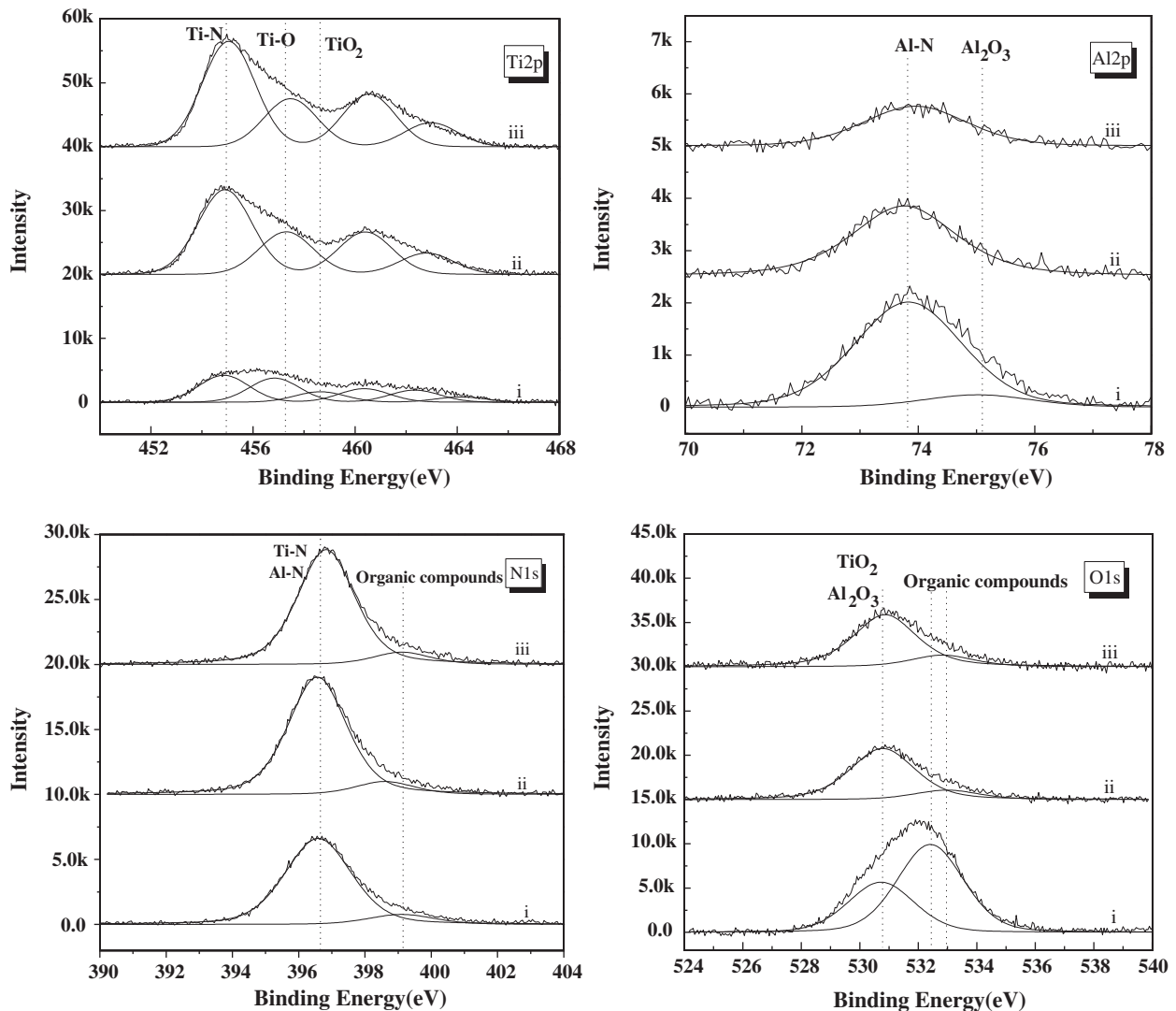

Fig. 4. XPS spectra of Ti2p, Al2p, N1s and O1s of the coating with $\lambda BD = 20$ nm: (i) no sputtering; (ii) sputtering for 20 min; (iii) sputtering for 27 min.

$\lambda_{BD} = 30$ nm, that meant they are multilayered in composition. The bright zone was abundant in Ti and the dark zone was abundant in Al. The overall thicknesses of the coatings are estimated to be about 749, 767, 820 and 785 nm, that correspond to the bilayer periods of about 4.8, 10.3, 18.0 and 25.4 nm, respectively.

XRD diffraction patterns from the coatings with different bilayer periods deposited onto TC4 substrates and from the bare substrate are shown in Fig. 3(a). The substrate displays mainly reflections from the α-Ti (PCPDF 44–1294). The crystal with strong (111) preferred orientation is the main texture of the coatings, which should belong to TiN or TiAlN (PCPDF 38–1420). Weak (220) and (222) reflections also present in some case. No obvious XRD patterns of AlN or Ti–Al intermetallic compounds were observed from the coatings. This can be explained by the reason that in Ti, Al and N system, because the heat formation of TiN (-305.6 kJ mol^{-1}) is lower than that of AlN (-241.6 kJ mol^{-1}), N preferentially combines with Ti to form TiN basic matter, and Al atoms just replace the partial Ti atoms in TiN crystal. So the (Ti, Al)N crystal still keeps TiN crystal structure, which is as similar as NaCl, only the lattice parameter decreases. The presence of (111) preferred orientation texture, which is often found in these type films fabricated by cathodic arc method, was caused by the condition of minimization of the overall film energy. The (111) plane in TiN or TiAlN is the one of the lowest strain energy due to the anisotropy in the Young's modulus and dominates the development of film. On the other hand, the energetic ions bombardment during deposition enhances the atoms migration rate and let them readily align along the densely packed direction, i.e. (111) direction.

Fig. 3(b) shows the fine XRD patterns around (111) peak from the coatings deposited onto Si wafers. There are some weak negative or positive satellite reflections (marked as S.R.) located on the both sides of the principal reflection (marked as P.R.), indicating that the coating has superlattice structure [19]. The bilayer periods estimated from the satellite reflections are around about 5.45, 11.13, 20.60 and 25.11 nm, respectively, being close to the values estimated from the SEM or the design.

EDS analysis results (not shown here) indicate that the main elemental composition of the coatings is of N, Ti and Al, and the atomic ratio of N:(Ti, Al) was about 1.24–1.29, meaning the coatings are overstoichiometric. Simultaneously, there are little O, V and Cr existing in the films. V and Cr should come from the cathode materials. The chemical binding states of the coatings were determined from XPS peaks of Ti2p$_{3/2}$, Al2p, N1s and O1s, which was calibrated with the binding energy of C1s (284.6 eV) in graphite. For each kind of XPS peak of Ti2p$_{3/2}$, Al2p, N1s or O1s recorded on the different samples, the shape is as similar as each other. A typical XPS spectral analysis is shown in Fig. 4 and Table 1. It indicates that on the coating surface, a mixture of TiN and/or TiAlN, Al$_2$O$_3$, TiO$_2$ and other titanium oxides (TiO$_x$), together with the amount of absorbed oxygen, organic compounds and carbon, is presented. Below the surface, in different layers, the contents of TiN or TiAlN increase but those of other compounds decrease, and no obvious aluminum oxides are observed in the inner. The rich aluminum oxide in the top layer undoubtedly provides better protection against the environment attack. The existing of TiO$_x$ in deep layer might because Ti is preferred to combine with O more than N for its higher activity. And at the same time, the relative contents of Ti and Al changed with the Ar$^+$ sputtering carried on, indicating that
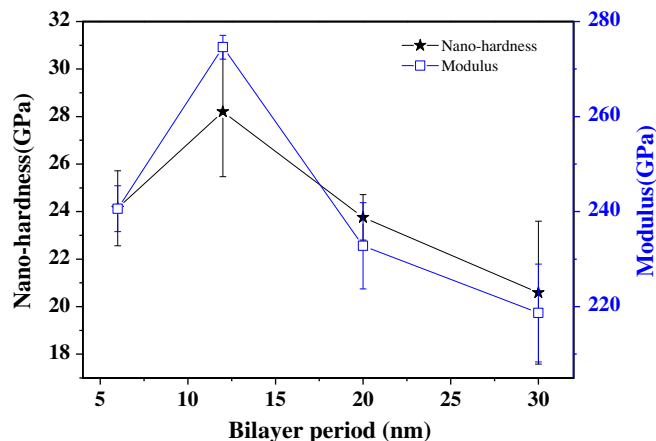

Fig. 5. Variation of nano-hardness and elastic modulus with bilayer period.

the coating composition distributes alternately. This result is in agreement with that concluded from SEM and XRD tests.

3.2. Mechanical performance of the coatings

The variation of nano-hardness and elastic modulus of the coatings on TC4 alloy substrates with bilayer period changing is shown in Fig. 5. They both increase, firstly, and then decrease while the bilayer period increases. The peak nano-hardness and modulus occur at $\lambda_{BD} = 12$ nm and the maximums are approximately 28 GPa and 283 GPa, respectively. These values were lower than that reported in reference [19]. This might be induced by the similar shear modulus of the individual layers of TiN and TiAlN [12]. Additionally, wide interfaces between the adjoining layers of heterogeneity may exist and decreased the inner strain, which contributed to hardness [23].

The as-prepared coatings are well adherent to the TC4 alloy substrates confirmed by the scratch tests, and the critical load is in the range from 33 N to 57 N. This consequence was obtained by the thin buffer layer of TiAl alloy providing a smooth transition in stress and hardness from substrate material to the coating. In addition, the pretreatment (cleaning bombardment of energetic ions) for the substrates prior to the deposition of the intermediate metallic layer of TiAl was beneficial to the adherent strength [20].

3.3. Corrosion resistance of the coatings

Potentiodynamic measurements generated a series of polarization curves of potential (relative to SCE) vs. current density, are presented in Fig. 6. Comparing to the corrosion potential ($E_{corr.}$) of the bare TC4 alloy (-0.397 V), E_{corr} was effectively increased by applying TiN/TiAlN multilayered coating. Especially for the coating with $\lambda_{BD} = 20$ nm, it reached $+0.310$ V vs. SCE. This increase represents a more notable electrode potential being achieved, thus indicating the improvement of corrosion resistance of TC4 alloy with these coatings. The remarkable corrosion resistance for the coating with $\lambda_{BD} = 20$ nm could be related to its dense columnar grain and intact nanometer periodic structure.

Table 1
The binding energies (in eV) of the XPS peaks and the corresponding phases.

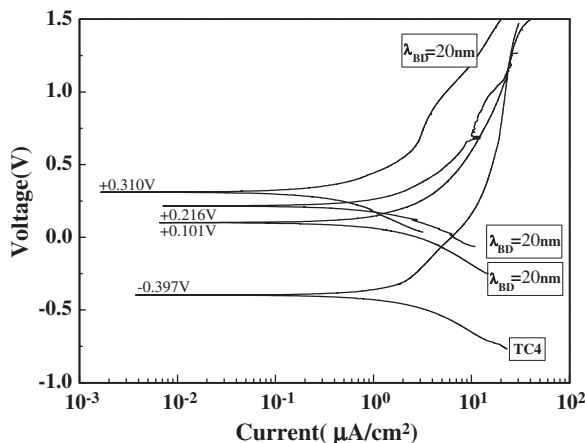| Condition	Ti2p$_{3/2}$			Al2p		N1s		O1s		
	Ti–N	TiO$_x$	TiO$_2$	Al–N	Al$_2$O$_3$	Ti–N Al–N	C–N bonds	Ti–O Al–O	C–O bonds
No sputtering	454.9	456.9	458.7	73.9	75.0	396.6	399.1	530.8	532.4
Sputtering for 21 min	454.9	457.3	–	73.8	–	396.6	398.6	530.8	533.0
Sputtering for 27 min	455.0	457.5	–	73.9	–	396.8	399.1	530.9	532.8

Fig. 6. Potentiodynamic polarization curves for bare TC4 alloy and the multilayered coatings with different bilayer periods on TC4 substrates in 5% aqueous NaCl solution.

4. Conclusions

TiN/TiAlN multilayer coatings with different bilayer periods in nanoscale were prepared on the TC4 alloy and Si (100) wafers by magnetic filtered pulsed vacuum cathodic arc plasma deposition method. The coatings are mainly consisted of TiN and (Ti, Al)N compounds with strong preferred orientation of (111), together with amounts of Titanium and/or aluminum oxides, especially in the surfaces. The atomic ratio of N:(Ti + Al) was about 1.24–1.29. A pre-treatment for substrate surface and an embedded buffer layer of TiAl alloy enhanced the adhesion strongly and the critical load is high to 57 N. The performance of the multilayer coating is affected by the bilayer periods remarkably. For nano-hardness and modulus, the highest values of 28 GPa and 283 GPa, respectively, were obtained from the coating with $\lambda_{BD} = 12$ nm. And for the resistance to chemical attack, the coating with $\lambda_{BD} = 20$ nm should work effectively. These results suggest that TiN/TiAlN multilayer coating with an appropriate bilayer period fabricated using this method may be more advantageous and has extensive applications.

References

[1] J. Pelleg, L.Z. Zevin, S. Lungo, N. Coritoru, Thin Solid Films 197 (1991) 117.
[2] M.B. Takeyama, A. Noya, K. Sakanishi, J. Vac. Sci. Technol. B 18 (3) (2000) 1333.
[3] I. Milošev, H.-H. Strehbtow, B. Navinšek, Thin Solid Films 303 (1997) 246.
[4] C. Liu, A. Leyland, Q. Bi, A. Matthews, Surf. Coat. Technol. 141 (2001) 164.
[5] V.N. Zhitomirsky, I. Grimberg, L. Rapoport, N.A. Travitzky, R.L. Boxman, S. Goldsmith, A. Raihel, I. Lapsker, B.Z. Weiss, Thin Solid Films 326 (1998) 134.
[6] N. Fateh, G.A. Fontalvo, G. Gassner, C. Mitterer, Wear 262 (2007) 1152.
[7] H. Ichimura, A. Kawana, J. Mater. Res. 8 (1993) 1093.
[8] J.H. Hsieh, C. Liang, C.H. Yu, W. Wu, Surf. Coat. Technol. 108–109 (1998) 132.
[9] M. Arndt, H. Westphal, Coatings in Manufacturing Processes 1–3 (2008) 151.
[10] S.J. Bull, D.G. Bhat, M.H. Staia, Surf. Coat. Technol. 163–164 (2003) 499.
[11] H.A. Jehn, B. Rother, Surf. Coat. Technol. 112 (1999) 103.
[12] J.S. Koehler, Phys. Rev. B 215 (1970) 547.
[13] P.C. Yashar, W.D. Sproul, Vacuum 55 (1999) 179.
[14] K.N. Andersen, E.J. Bienk, K.O. Schweitz, H. Reitz, J. Chevallier, P. Kringhøj, J. Bøttiger, Surf. Coat. Technol. 123 (2000) 219.
[15] S.G. Harris, E.D. Doyle, A.C. Vlasveld, P.J. Dolder, Surf. Coat. Technol. 146–147 (2001) 305.
[16] E. Altuncu, F. Üstel, Mater. Manufacturing Processes 24 (2009) 796.
[17] A. Madan, P. Yashar, M. Shinn, S.A. Barnett, Thin Solid Films 302 (1997) 147.
[18] W.-D. Münz, L.A. Donohue, P.Eh. Hovsepian, Surf. Coat. Technol. 125 (2000) 269.
[19] H.C. Barshilia, K.S. Rajam, Jain Anjana, K. Gopinadhan, Chaudhary Sujeet, Thin Solid Films 503 (2006) 158.
[20] P.Eh. Hovsepian, D.B. Lewis, Q. Luo, W.-D. Münz, P.H. Mayrhofer, C. Mitterer, Z. Zhou, W.M. Rainforth, Thin Solid Films 485 (2005) 160.
[21] V. Braic, C.N. Zoita, M. Balaceanu, A. Kiss, A. Vladescu, A. Popescu, M. Braic, Surf. Coatings Technol. 204 (2010) 1925.
[22] W. Aperador, J.C. Caicedo, C. Espa, G. Cabrera, C. Amaya, J. Phys. Chem. Solids 71 (2010) 1754.
[23] N.J.M. Carvalho, Thin Solid Films 429 (2003) 179.
[24] N.J.M. Carvalho, J.Th.M. De Hosson, Acta Materialia 54 (2006) 1857.
[25] R. Mientus, K. Ellmer, Surf. Coatings Technol. 116–119 (1999) 1093.
[26] C. Ducros, F. Sanchette, Surf. Coatings Technol. 201 (2006) 1045.